



OPEN ACCESS

EDITED BY

Gang Rao,
Southwest Petroleum University, China

REVIEWED BY

Xi Xu,
China Aero Geophysical Survey and
Remote Sensing Center for Natural
Resources, China
Yangwen Pei,
China University of Petroleum, Huadong,
China

*CORRESPONDENCE

Jin-Hyuck Choi,
✉ cjh9521@kigam.re.kr

RECEIVED 10 March 2023

ACCEPTED 25 May 2023

PUBLISHED 05 June 2023

CITATION

Cheon Y, Shin YH, Park S, Choi J-H,
Kim D-E, Ko K, Ryoo C-R, Kim Y-S and
Son M (2023), Structural architecture and
late Cenozoic tectonic evolution of the
Ulsan Fault Zone, SE Korea: New insights
from integration of geological and
geophysical data.
Front. Earth Sci. 11:1183329.
doi: 10.3389/feart.2023.1183329

COPYRIGHT

© 2023 Cheon, Shin, Park, Choi, Kim, Ko,
Ryoo, Kim and Son. This is an open-
access article distributed under the terms
of the [Creative Commons Attribution
License \(CC BY\)](https://creativecommons.org/licenses/by/4.0/). The use, distribution or
reproduction in other forums is
permitted, provided the original author(s)
and the copyright owner(s) are credited
and that the original publication in this
journal is cited, in accordance with
accepted academic practice. No use,
distribution or reproduction is permitted
which does not comply with these terms.

Structural architecture and late Cenozoic tectonic evolution of the Ulsan Fault Zone, SE Korea: New insights from integration of geological and geophysical data

Youngbeom Cheon¹, Young Hong Shin¹, Samgyu Park²,
Jin-Hyuck Choi^{1*}, Dong-Eun Kim¹, Kyoungtae Ko³,
Chung-Ryul Ryoo¹, Young-Seog Kim⁴ and Moon Son⁵

¹Active Tectonics Research Center, Korea Institute of Geoscience and Mineral Resources, Daejeon, Republic of Korea, ²Mineral Exploration and Mining Research Center, Korea Institute of Geoscience and Mineral Resources, Daejeon, Republic of Korea, ³Geological Research Center, Korea Institute of Geoscience and Mineral Resources, Daejeon, Republic of Korea, ⁴Major of Environmental Geosciences, Pukyong National University, Busan, Republic of Korea, ⁵Department of Geological Sciences, Pusan National University, Busan, Republic of Korea

Integration of geological and geophysical data is essential to elucidate the configuration and geometry of surface and subsurface structures, as well as their long-term evolution. The NNW–SSE-striking incised valley and parallel mountain range in the southeastern margin of the Korean Peninsula, extending 50 km from Gyeongju to Ulsan cities, are together regarded as one of the most prominent geographical features in South Korea. This paper presents an investigation into the structural architecture and deformation history of the valley and mountain range during the late Cenozoic based on combined data from field observations and gravity and electrical resistivity surveys. Our results based on integrated and reconciled geological, structural, and geophysical data are as follows. First, the incised fault valley can be divided into 1) the northern part, which comprises several distributed buried or exposed fault strands; and 2) the southern part, which comprises a concentrated deformation zone along the eastern margin of the valley. Different deformation features between the two parts are controlled by the lithology of host rocks and by the location and geometry of the neighboring major structures, that is, the Yeonil Tectonic Line (YTL) and the Yangsan Fault. Second, we defined the Ulsan Fault Zone as a NNW–SSE-to N–S-striking fault within the incised valley and along the eastern margin of the valley. In particular, the constituent strands located along the eastern margin of the valley have acted mainly as an imbricate thrust zone, characterized by an east-side-up geometry with moderate to low dip angles and reverse-dominant kinematics in the shallow subsurface during the Quaternary. Third, reactivated strands within the Ulsan Fault Zone during the Quaternary are interpreted as shortcut faults developed in the footwall of Miocene subvertical structures, predominantly the YTL. In addition, movements on the Ulsan Fault Zone and the YTL during the Miocene to Quaternary were arrested by the NNE–SSW-striking Yangsan Fault, which was a prominent and mature pre-existing structure. Our results highlight the spatiotemporal structural variation in SE Korea and emphasize the strong control of the configuration and geometry of pre-existing structures on the distribution and characteristics (i.e., geometry

and kinematics) of the subsequent deformation under changing tectonic environments through the late Cenozoic.

KEYWORDS

Ulsan Fault, gravity and electrical resistivity surveys, Yeonil Tectonic Line, pre-formed structure, Cenozoic crustal deformation

1 Introduction

The Korean Peninsula is situated in the eastern continental margin of Eurasia and has been an important tectonic link between eastern China and the Japanese arc during the Cenozoic (Chough et al., 2000; Chough and Sohn, 2010; Son et al., 2015). The time-dependent stress fields and resultant crustal deformation in and around the peninsula during the Cenozoic have been controlled by the relative tectonic motion between the Eurasia, Pacific, and Philippine Sea plates (Figure 1A) as well as the Indian plate (e.g., Engebretson et al., 1985; Lithgow-Bertelloni and Richards, 1998; Hall, 2002; Yin, 2010; Xu et al., 2021). The Miocene back-arc opening of the East Sea (Sea of Japan) between the Korean Peninsula and the Japanese Arc was a prominent late Cenozoic geological event in eastern Asia (e.g., Jolivet et al., 1994; Chough et al., 2000; Taira, 2001). At that time, strike-slip- and extensional-faulting-related crustal subsidence and also dacitic to basaltic volcanic activity occurred pervasively in the southeastern Korean Peninsula (Figure 1B; e.g., Son et al., 2002, 2005, 2013, 2015; Sohn et al., 2013; Yoon et al., 2014). Subsequently, neotectonic activity (since ~5 Ma to present) expressed as strike-slip to contractional deformation, has been concentrated mainly along pre-existing major structures in SE Korea (Figure 1B; e.g., Park et al., 2006; Choi et al., 2012; Lee et al., 2011; Kim et al., 2016; Cheon et al., 2020a, b; Ha et al., 2022; Kim et al., 2021c; Ko et al., 2022; Lee et al., 2022).

In the southeastern margin of SE Korea, the NNW–SSE-striking mountain/hill range and adjacent parallel western valley (>2 km wide and ~50 km long) have together long been regarded as one of the most active structures in the Korean Peninsula (Figure 1C; e.g., Kyung, 1997; Okada et al., 1998; Ryoo et al., 2002; Choi, 2003). The range includes Mt. Tohamsan (745 m), Mt. Jinjeonsan (411 m), Mt. Baekilsan (560 m), Mt. Gwanmunsan (640 m), Mt. Dongdaesan (446 m), and Mt. Muryongsan (450 m), from north to south. Paleoseismic and structural investigations along the western front of the mountain range, which is composed mostly of alluvial fans, show records of reverse faulting during the late Quaternary, characterized by several NNW–SSE-to N–S-striking fault strands and top-to-the-west kinematics (Figure 1C; e.g., Song and Kyung, 1996; Okada et al., 1998; Chang, 2001; Choi, 2003; Ryoo et al., 2002; Ryoo, 2009; Choi et al., 2014, 2015; Kim et al., 2021c; Gwon et al., 2021; Naik et al., 2022; Park et al., 2022). The geomorphic feature of the western valley has been interpreted as an incised fault valley (Figure 1C; Kim, 1973; Kim et al., 1976; Kang, 1979a and b), although no clear field evidence has been presented for faults within the valley itself. Indeed, it is not easy to detect faults owing to thick sedimentary cover, land cultivation, and urbanization (Ulsan and Gyeongju cities; e.g., Choi, 2003). Ulsan City, in the southern part of the valley (Figure 1C), is the largest industrial city in South Korea and has several national facilities and industrial complexes, and Gyeongju City, in the northern part of the

valley (Figure 1C), is one of the ancient capital cities of South Korea and has many cultural assets. For these reasons, the possible existence and geometry of faults, as well as their long-term movement history and the possibility of future earthquakes, have been raised as important socio-scientific issues during the last few decades.

Despite the scientific and socio-economic interest in faults in the valley, unresolved questions remain concerning the existence, geometry, evolution, and kinematics of these faults. First, the definition of the main fault remains uncertain and controversial. Several studies conducted during the 1970s termed the main structural feature aligned with the NNW–SSE-striking incised valley the “Ulsan Fault” (e.g., Kim, 1973; Kim et al., 1976; Kang, 1979a and b), but several subsequent studies adopted the term “Ulsan Fault Zone” to describe the various mapped and inferred NNW–SSE-to N–S-striking fault strands in and around the incised valley (e.g., Ryoo et al., 2000, 2001, 2002, 2004; Ryoo, 2009; Lee et al., 2018). However, Okada et al. (1998) used the term “Ulsan Fault System” to describe NNW–SSE-striking neotectonic reverse faults that were mapped along the western front of the mountain range. Choi (2003) defined the incised valley and its eastern reverse-fault traces together as the “Ulsan Fault System”. Kee et al. (2019) proposed that only the reverse-fault traces exposed along the western front of the mountain range should be referred to as the “Ulsan Fault”. Second, the nature and extent of geometric connectivity among adjacent major faults are also unclear. The spatiotemporal relationship between the Yeonil Tectonic Line (YTL; Figures 1B, C), which is the western boundary fault of the Miocene crustal deformation (e.g., Son et al., 2002, 2013, 2015), and the Ulsan Fault remains uncertain (Choi et al., 2015). In addition, the characteristics of deformation within the λ -shaped intersection area (Du and Aydin, 1995; Kim et al., 2000) of the NNE–SSW-striking Yangsan Fault and the NNW–SSE-striking Ulsan Fault (Park, 2004; Han et al., 2017) are also unclear (Figures 1B, C). Third, the evolution of the Ulsan Fault during the pre-neotectonic stage, including kinematics and movement ages, remains poorly constrained. The fact that these questions remain unresolved is because of limitations in mapping fault geometry and investigating fault-zone architecture as a result of sediment cover obscuring the Ulsan and other faults.

To reveal buried structures in the study area, it is necessary to obtain various types of geophysical data and reconcile interpretations of these data with field observations. The primary purpose of this study is to establish the geometrical features of the main NNW–SSE-striking faults of SE Korea and reexamine their long-term evolution and active faulting mechanism on the basis of results from our new geophysical surveys and field investigations. In this study, we describe distribution, geometry, and kinematics of the exposed faults along the mountain range based on field observations. We then present the existence and distribution of subsurface

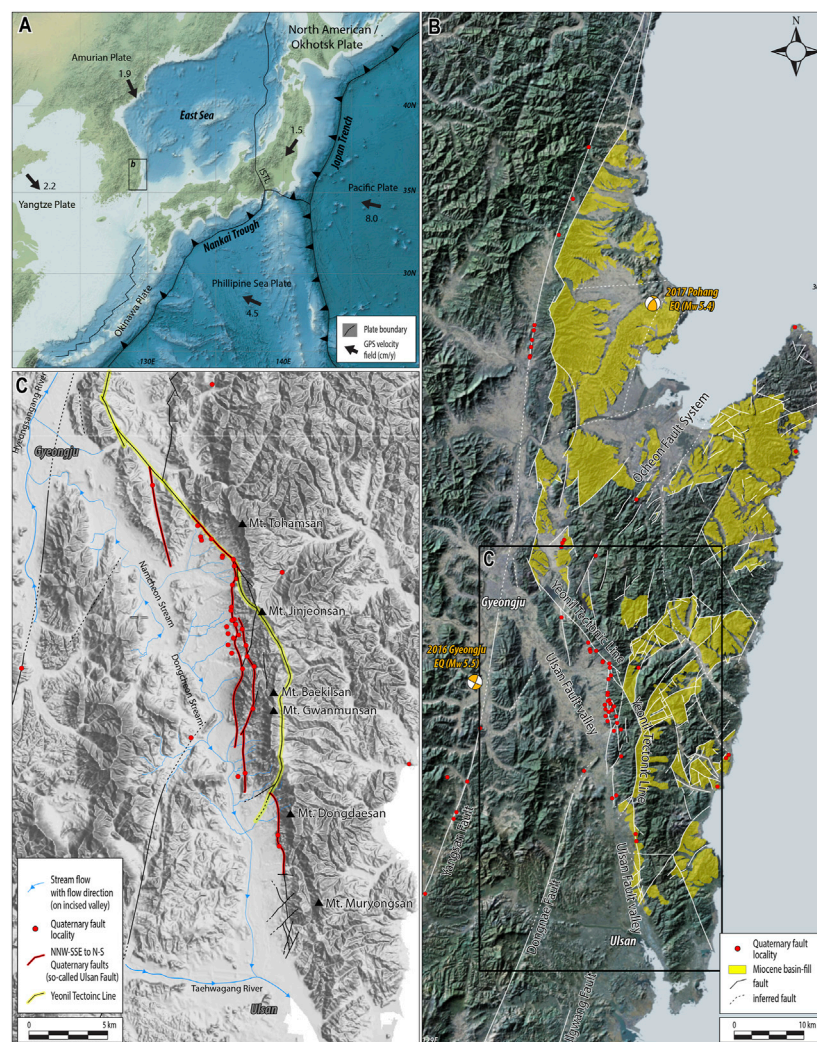


FIGURE 1

(A) Map of the present-day tectonics of eastern Asia, showing plates and their velocities (modified from Schellart and Rawlinson, 2010). The velocities of the plates are based on the Indo-Atlantic hotspot reference frame of O'Neill et al. (2005) and the relative plate motion model of DeMets et al. (1994). (B) Map of the distribution of the main faults and Miocene basin-fills in the southeastern margin of the Korean Peninsula (modified from Son et al., 2015) and Quaternary fault outcrops. (C) Map of the distribution of NNW–SSE-to N–S–striking faults in the incised valley–mountain range of SE Korea.

structures within the incised valley using gravity and electrical resistivity surveys and define the overall geometry of the main NNW–SSE-striking faults in SE Korea. We also propose a new definition of the “Ulsan Fault Zone” and discuss the spatiotemporal evolution of this fault during the late Cenozoic, as well as its relationships with adjacent major structures.

2 Geological and tectonic background

During the late Cenozoic, several major plate reorganizations in and around Asia related with continental collision and oceanic subduction have produced various types of intracontinental deformation in Korea (e.g., Yin, 2010; Cheon et al., 2019; Xu et al., 2021; Lee et al., 2022). In the late Oligocene to early Miocene, back-arc opening of the East Sea commenced (e.g.,

Jolivet et al., 1994; Chough et al., 2000; Taira, 2001) and a number of the Miocene sedimentary basins related to the East Sea opening were formed along the coastal areas in southeast margin of Korea. The immature basins on land were mainly controlled by dextral-slip and normal-slip movements of the NNW–SSE-striking (e.g., the YTL) and NNE-SSW- to NE–SW-striking faults (e.g., Ocheon Fault System), respectively (Figure 1B; e.g., Son et al., 2002, 2005, 2013, 2015; Cheon et al., 2012; Kim et al., 2020a). At about 16 Ma, the subduction of the Philippine Sea plate beneath the Japanese Islands caused inversion of the Miocene basins along with the formation of some contractional to strike-slip structures under a NNW–SSE maximum horizontal stress (e.g., Fabbri et al., 1996; Lee et al., 1999; Kim et al., 2008a; Son et al., 2013, 2015; Cheon et al., 2019).

Since ~5 Ma, the neotectonic stress regime of the Korean Peninsula is controlled by a combined effect of the westward-

shallowing subducting Pacific plate and the northwestward high-angle subducting Philippine Sea plate beneath the Eurasia plate, as well as the far-field stress of the India–Eurasia collision (Figure 1A; e.g., Park et al., 2006; Kim et al., 2016; Kuwahara et al., 2021; Kim et al., 2023). It has been reconstructed as ENE–WSW (N70°–75°E-trending) maximum horizontal stress from Quaternary fault slip data, earthquake focal mechanisms, and *in situ* drilling (hydrofracturing and overcoring) data (e.g., Park et al., 2006; Kim et al., 2016; Kim et al., 2021a; Kuwahara et al., 2021). During this period, Korea has been regarded as a seismically stable area compared with neighboring countries, such as Japan and China (Figure 1A), based on the absence of damaging earthquakes in modern history prior to the occurrence of two recent moderate earthquakes (the 2016 M_w 5.5 Gyeongju and 2017 M_w 5.4 Pohang earthquakes; Figure 1B). However, together with these two recent moderate-sized earthquakes, geological records of paleo-earthquakes reveal that neotectonic crustal deformation is spatially distributed over the entire Korean Peninsula.

The southeastern part of the peninsula is known to have been the most active part during the neotectonic period and contains several major structures (the Yangsan Fault System, Ulsan Fault, and border faults of Miocene sedimentary basins, including the YTL and Ocheon Fault System), as well as pervasively distributed smaller faults (Figure 1B; e.g., Chang and Chang, 1998; Choi et al., 2009, 2012; Cheon et al., 2012, 2019, 2020a, b; Son et al., 2013, 2015; Kim et al., 2016, Kim et al., 2020a; Kim et al., 2021b and c). The NNE–SSW-striking Yangsan Fault has evolved as a long-lived, crustal-scale mature fault during multiple deformation stages since the Late Cretaceous, and some sections have been reactivated under the current stress field (Figure 1B; e.g., Cheon et al., 2019, 2020a, b; Kim et al., 2023; Ha et al., 2022; Ko et al., 2022). To the east of the Yangsan Fault, some sections of the Miocene faults show records of neotectonic deformation (Figure 1B; e.g., Cheong et al., 2003; Choi et al., 2015; Son et al., 2015). These old structures and their partial reactivation indicate that neotectonic deformation in SE Korea is accommodated primarily along the long-lived inherited structures. Kim et al. (2023) proposed that reactivation of the relatively misoriented pre-existing faults, accommodating mainly transpressional deformation, was controlled by factors including mantle-derived fluids, heat flow, and lithospheric structures.

3 Geomorphic and structural features along the incised valley–mountain range

In here, we reexamine the distribution, geometry, and kinematics but also internal structures of the buried and exposed faults along the incised valley and mountain range based on a compilation of early works and our new observations.

3.1 Fault evidences along the incised valley

During the 1970s, several studies regarded the incised valley as a major structure, as inferred from the presence of a distinct linear

arrangement of fluvial landforms (e.g., Kim, 1973; Kim et al., 1976; Kang, 1979a and b) and terms this valley the “Ulsan Fault”. Subsequently, because of the lack of topography and outcrops due to erosional processes and human activity, several geophysical surveys along some sections or areas of the valley were conducted to detect subsurface structures and to estimate their neotectonic activity (e.g., Lee and Um, 1992; Baag and Kang, 1994; Shon et al., 1999; Lee et al., 2000; Kim et al., 2008b). Of these studies, the results of the cross-valley high-frequency magnetotelluric (MT) survey conducted by Shon et al. (1999) suggested that the eastern and western marginal parts of the valley are highly deformed relative to the central part. Electrical (seismic refraction and reflection) surveys and gravity measurements conducted by Kim et al. (2008b) revealed several moderate-to steep-dipping anomalies, which were regarded as constituent structures of the fault-zone valley, as well as some buried faults that cut the unconsolidated sediments, as interpreted from smoothed refraction velocity tomograms and stacked sections. However, neotectonic activity detected only by geophysical surveys remains subject to verification (e.g., Choi et al., 2002) because of the lack of ground excavation and drilling surveys to confirm movement on faults.

Our geomorphic analysis on drainage networks of the incised valley shows a particular geomorphic feature (Figure 1C) whereby in contrast to most incised valleys, which constitute only one main trunk, the valley in the study area has two main streams (the Namcheon and Dongcheon streams) that flow in different directions, respectively. The Namcheon Stream originates in Mt. Tohamsan and flows to the north-northwest, where it joins the Hyeongsan River that flows north-northeastward along an incised valley of the Yangsan Fault. In comparison, the Dongcheon Stream flows south-southeastward along the valley, joins the Taehwagang River, and flows into the East Sea. The divide of the two main streams is in the central part of the incised valley (Figure 1C). In addition, numerous borehole data from the Geotechnical Information Database system (<https://www.geoinfo.or.kr/>) collated by the Korean Ministry of Land, Infrastructure, and Transport show that thicknesses of unconsolidated strata within the valley are greater than 30 m and that some local areas display abrupt variations in strata thickness.

3.2 Fault characteristics along the mountain range

Along the eastern margin of the valley (i.e., the western front of the mountain range), a number of fault outcrops have been identified, some of which show that the fault cuts young unconsolidated sediments (Figure 1C; Table 1). In outcrops, trench walls, and drilling surveys, the faults show typical reverse-slip features, such as east-side-up apparent offset, drag pattern, and flat-ramp geometry (e.g., Ryoo et al., 2001, 2002, 2004; Choi et al., 2002, 2003; Park et al., 2020; Kim et al., 2021c; Gwon et al., 2021; Naik et al., 2022; Park et al., 2022). The fault strands are featured by slightly curved multiple strands (generally NNW–SSE to N–S), which anastomose and link up with each other. They dip toward the east at moderate to low angles; however, at some sites, they have been rotated to trend NNE–SSW or NW–SE and dip at high angles (Figures 2A–D; Table 1). In addition, west-dipping antithetic faults are locally observed (Figure 2D; Table 1). Fault kinematics confirmed mostly at outcrops are reverse-slip with a secondary component of dextral-slip, but dextral-slip is predominant at some sites. Although fault

TABLE 1 Information reported by previous studies on slip data for active fault surfaces at each site along the western front of the mountain range.

No.	Site name	Strike	Dip	Kinematics	Location (latitude, longitude)	References
1	Madong1	021	31	R+RL	35.800528 129.315778	Choi et al. (2012)
2	Madong2	356	42	R+RL	35.792472 129.318267	Choi et al. (2012)
3	Madong3	335	56	R+RL	35.792369 129.318292	Choi et al. (2012)
4	Tabgol	356	42	R+RL	35.792892 129.324600	Choi et al. (2012)
5	Jinhyun1	355	68	R+RL	35.782994 129.331769	Choi et al. (2012)
6	Jinhyun2	328	65	RL+R	35.783333 129.331928	Choi et al. (2012)
7	Jinti	328	80	R+RL	35.782997 129.331817	Choi et al. (2012)
8	Singye	303	27	R+RL	35.777556 129.339500	Choi et al. (2012)
9	Geiryung	030	30	R+RL	35.767139 129.337833	Choi et al. (2012)
10	Hwalseong	353	65	RL+R	35.754975 129.336936	Choi et al. (2012)
11	Malbang1	309	44	R	35.747406 129.337028	Choi et al. (2012)
12	Malbang2	334	40	R	35.741861 129.342167	Choi et al. (2012)
13	Malbang3	342	42	R	35.752964 129.336475	Choi et al. (2012)
14	Jeolgol1	340	43	R	35.748081 129.338294	Choi et al. (2012)
15	Jeolgol2	352	28	R	35.745161 129.339214	Choi et al. (2012)
16	Jeolgol3	350	80	R	35.741861 129.339161	Choi et al. (2012)
17	Sagok1	350	62	RL+R	35.747458 129.337267	Choi et al. (2012)
18	Sagok2	355	38	RL+R	35.746814 129.337869	Choi et al. (2012)
19	Tabbeon1	350	30	RL+R	35.744036 129.333406	Choi et al. (2012)
20	Tabbeon2	350	30	RL+R	35.740236 129.334167	Choi et al. (2012)
21	Gaegok1	172	88	RL+R	35.733917 129.334194	Choi et al. (2012)
22	Gaegok2	330	72	RL+R	35.737872 129.337231	Choi et al. (2012)
23	Gaegok3	334	40	R	35.739028 129.340222	Park et al. (2006)
24	Gaegok4	325	42	LL+R	35.742333 129.343386	Choi et al. (2012)
25	Gaegok5	025	55	R+RL	35.736639 129.336833	Choi et al. (2012)
26	Gaegok6	178	45	R	35.729278 129.336306	Choi et al. (2012)
27	Gaegok7	022	86	RL+R	35.737000 129.337278	Choi et al. (2012)
28	Gaegok8	342	88	R+RL	35.740000 129.341639	Choi et al. (2012)
29	Ipsil	348	75	R+RL	35.721575 129.351108	Choi et al. (2012)
30	Wonwonsa1	164	52	R+RL	35.697361 129.350778	Kim et al. (2021b)
31	Wonwonsa2	221	38	RL+R	35.697914 129.350959	Kim et al. (2021c)
32	Mohwa	303	45	RL+R	35.684594 129.341680	Choi et al. (2012)
33	Ihwa	8	74	R	35.662056 129.344500	Choi et al. (2012)
34	Hwajeong	0	20	-	35.659556 129.340611	Choi et al. (2012)
35	Bokgol	178	58	R	35.636972 129.371556	Lee. (2003)
36	Chail1	349	22	R	35.621472 129.369667	Choi et al. (2012)
37	Chail2	334	50	RL+R	35.621339 129.369561	Gwon et al. (2021)



FIGURE 2

(A) Photograph of the Quaternary fault exposure at the Madong 2 site (Table 1), showing Quaternary conglomerate thrust by Paleogene granite, and (B) close-up photograph of part of the exposed outcrop. (C) Trench photograph showing the Quaternary fault at the Chail 2 site (from Gwon et al., 2021; Table 1). (D) Attitude and kinematics of Quaternary movements on the NNW–SSE-striking faults. Rake is defined as the direction of slip motion with respect to the strike, measured from the horizontal line. Values are between -180° and 180° (left-lateral slip: near 0° ; right-lateral slip: near 180° ; normal: near -90° ; reverse: near 90°). The “Max” value is the percentage of data in the largest histogram bar. (E) Pervasively damaged and altered granites along a NNW–SSE-striking segment of the YTL. (F) A NNE–SSW-striking subsidiary fault of the YTL showing ~ 2 m-thick breccia zone.

spays observed at outcrops cutting the unconsolidated sediments are expressed as slip zones measuring a few centimeters wide (Figure 2B), the adjacent basement rocks are pervasively deformed and altered and are presumed to be pre-neotectonic deformation.

Meanwhile, the YTL is located <3 km east of the reverse-slip fault traces. The structure is a major strike-slip fault zone that controlled Miocene crustal deformation and basin formation (Figures 1B, C; Kim et al., 1998; Son et al., 2002, 2013, 2015). It is composed of NNW–SSE-, N–S-, and NNE–SSW-striking segments. The NNW–SSE- to N–S-striking subvertical segments with dextral-slip kinematics acted as a principal displacement zone, and the NNE–SSW-striking segment ($>75^{\circ}$ dip to the east) with oblique-to normal-slip kinematics acted as a releasing bend during the Miocene (Figure 1B, C; Son et al., 2002, 2013, 2015). The faults appear as pervasively brecciated, fractured, and hydrothermally altered zones measuring several tens of meters wide with high-angle dips (Figures 2E, F).

4 Gravity survey and data analysis

Gravity surveys can be used to detect subsurface discontinuities, across which there is a high material density difference, and they can

therefore be used to trace buried faults (e.g., Blakely, 1995; Saltus and Blakely, 2011; Wada et al., 2017). Such surveys are able to investigate the general distribution and geometry of large faults in a short time at low cost, although there are limitations regarding resolution on the detection of detailed internal structures of fault zones. To reveal the map-scale characteristics of the fault zone in the study area, we conducted a gravity survey of the NNW–SSE-trending incised valley–mountain range.

4.1 Data acquisition and processing

The Korea Institute of Geoscience and Mineral Resources (KIGAM) has been conducting gravity research since the late 1960s and played an important role in establishing Korea’s early gravity reference network and exploring geological structures. After 2000, KIGAM acquired gravity data using a Global Navigation Satellite System, which yields more accurate positioning than previous classical surveys, for the purpose of regional mapping covering the whole of South Korea (Lim et al., 2019). These gravity data include exploration data on the epicenters of the 2016 Gyeongju (M_w 5.5) and 2017 Pohang (M_w 5.5) earthquakes

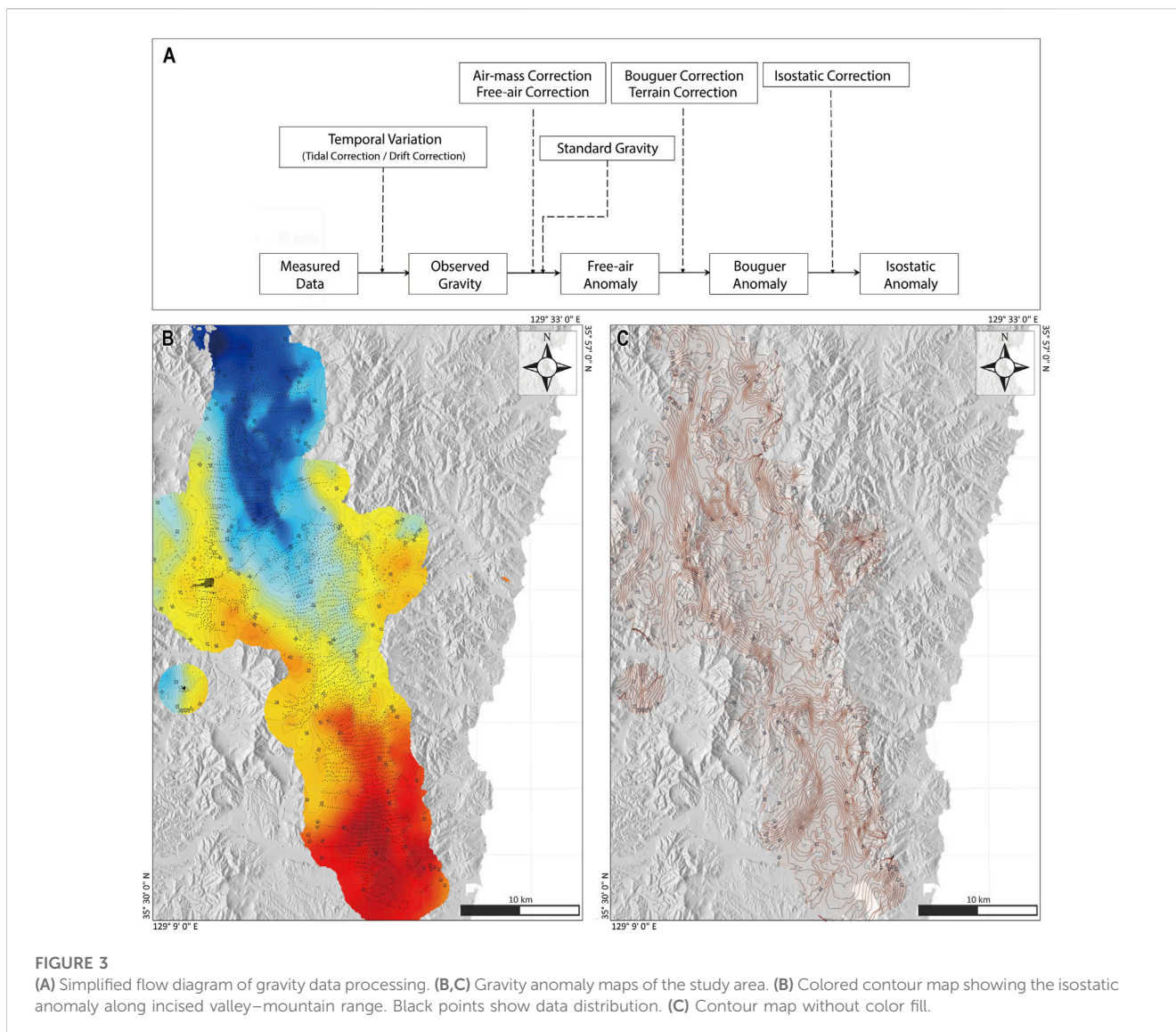


(Figure 1B). Recently, KIGAM conducted gravity measurements on major fault zones in SE Korea (Lee, 2020; Choi, 2021). In this study, we present a gravity anomaly map of the incised valley–mountain range of SE Korea (Figures 3B, C).

Figure 3A presents a sequence showing data acquisition and processing of our gravity survey. To identify faults in the shallow crust, we used isostatic anomalies with the effect of the Moho topography removed. Isostatic anomalies (Figures 3B, C) were determined by calculating the observed gravity, with the temporal change in gravity and random errors removed by tidal correction and network adjustment, and then performing gravity corrections; i.e., air-mass, free-air, Bouguer, terrain, and isostatic corrections (Choi et al., 2003; Lim et al., 2019). To calculate the gravity effect due to topography, SRTM3 (digital topography data from the three-arc-second Shuttle Radar Topography Mission; Farr et al., 2007) and SRTM30_plus (Becker et al., 2009) were used, and for isostatic correction, equal mass was assumed for the compensation depth in the Airy–Heiskanen model (Heiskanen and Vening Meinesz, 1958).

Tracing faults using gravity measurements has generally been applied to subvertical or vertical faults. If the difference in density between the two sides of a fault occurs as a result of shear displacement, then it is expressed in the form of a stepped gravity anomaly, and the midpoint of the step can be assumed to indicate the location of the fault (e.g., Blakely, 1995; Saltus and Blakely, 2011; Wada et al., 2017). Lee (2020) and Choi (2021) reported another type of gravity anomaly, which shows an elongated lineament structure in the form of a narrow U-shaped valley (trough shape in cross-sectional view) along the Yangsan Fault. Those authors interpreted the shape of the anomaly as having been produced by mechanical and/or chemical weakening processes along the fault deformation zone (e.g., wide fault core and/or damage zones, and flower structures of strike-slip faults), resulting in low-gravity-anomaly lineaments. Those authors resultantly classified the former step-shape gravity anomaly as type I and the latter U-shape gravity anomaly as type II. Type I is common not only in fault structures but also along various geological

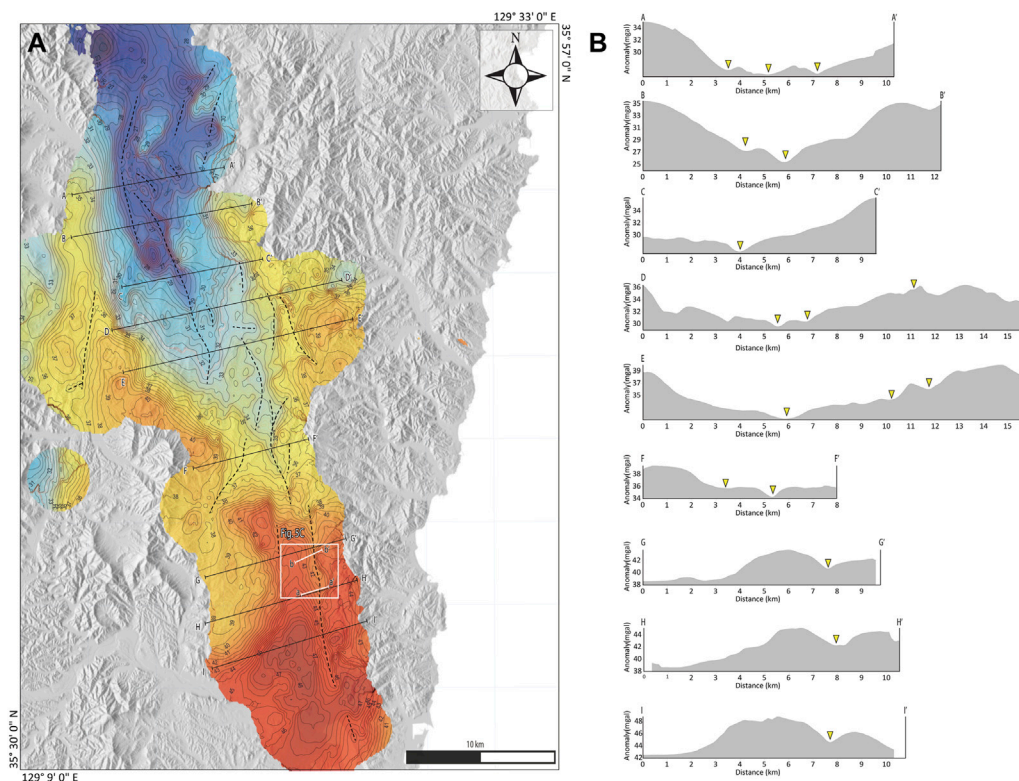


FIGURE 4

(A) Gravity lineaments interpreted as type II anomalies, shown as dashed black lines (see Section 4.1 for the definition of “type II” anomalies). Solid black and white lines indicate reference lines of cross-section profiles of gravity (B) and electrical resistivity anomalies (Figure 5A), respectively. (B) Across-fault cross-sections of gravity anomalies. Yellow triangles indicate buried or exposed fault structures.

boundaries with density differences, whereas type II is related mainly to fault boundaries.

4.2 Results and interpretation

Figure 4A shows a gravity anomaly map of the study area and the distribution of gravity lineaments interpreted as type II (shown U-shape gravity anomalies described as yellow triangles in Figure 4B). The gravity anomaly pattern shows relatively high gravity anomalies in the southern part of the study area (Ulsan area), whose bedrock is composed mostly of Cretaceous sedimentary rocks. In contrast, the pattern shows relatively low gravity anomalies in the northern part (Gyeongju area), whose bedrock consists of Late Cretaceous to Paleogene granitic rocks. The approximate densities of the older sedimentary and younger granitic rocks are 2,690 and 2,600 kg/m³, respectively (Sohn et al., 2020, and references therein). In the southern part of the study area, a N–S-directed localized anomaly is located along the eastern marginal part of the valley and corresponds to an exposed Quaternary fault trace (Figure 4), in contrast to the pervasively distributed connected or disconnected anomalies in the northern part of the study area. The location of the gravity anomaly observed along the eastern marginal area of the valley also corresponds to a zone of Quaternary fault traces observed in the field (Figure 4). Of the anomalies distributed within the northern part of the study area, the westernmost anomaly (Figure 4)

extends to the NNE–SSW and is regarded as corresponding to the Yangsan Fault, which shows a λ-type geometry in plan view. Although there were insufficient stations to detect structures in the mountain range, a roughly identified NNW–SSE-to N–S-trending anomaly shows considerable overlap with the trace of the YTL. The southern part of the YTL extends to the southwest and acts as a boundary between the southern part of the valley, which contains a localized anomaly, and the northern part of the valley, which is characterized by several anomalies (Figure 4).

The similarities between the gravity map and geological images of the distribution of faults indicate several map-scale subsurface geological structures in the study area and also support the existence of previously reported structures, such as Quaternary reverse-fault traces and the YTL observed in the mountain range.

5 Electrical resistivity survey and data analysis

The electrical resistivity method utilizes differences in electric potential to identify the electrical properties of subsurface materials. In general, a fault zone, which is characterized by incohesive fault rocks and distributed fractures owing to brittle deformation, has lower resistivity relative to surrounding rocks, meaning that electrical resistivity surveys are useful for detecting and tracing subsurface faults. We conducted an electrical resistivity survey

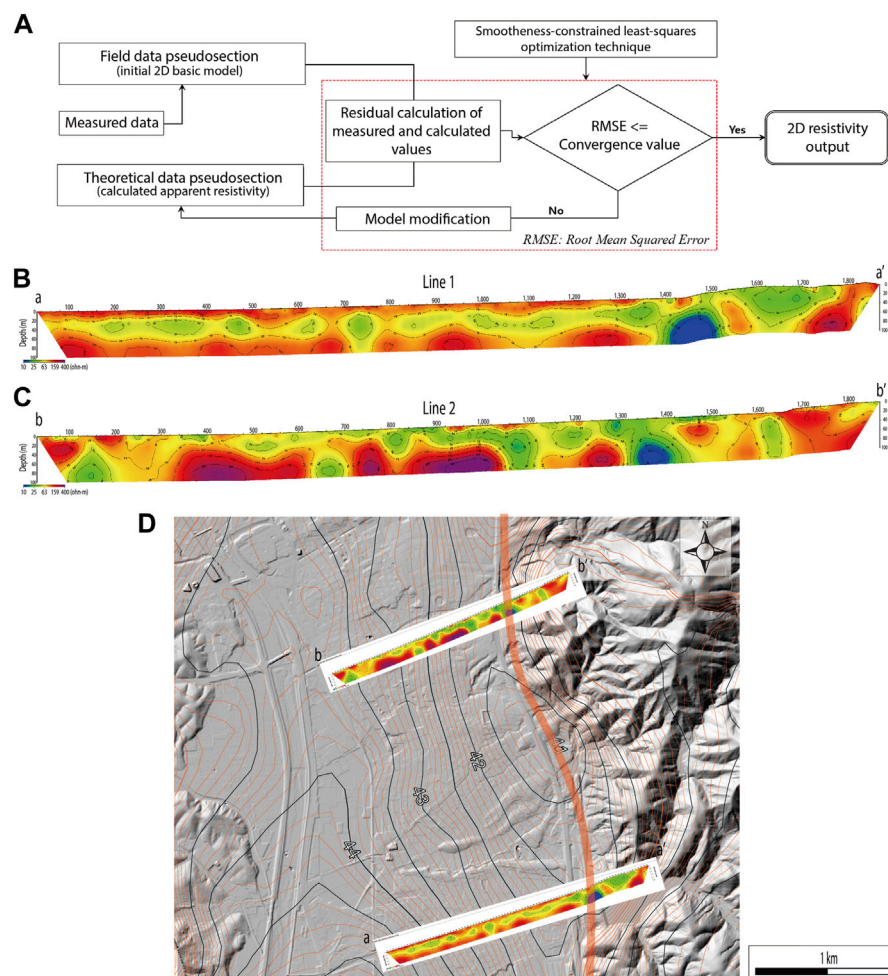


FIGURE 5

(A) Simplified flow diagram of electrical resistivity data processing. Across-fault survey line 1 (a–a') (B) and survey line 2 (b–b') (C) cross-sections of electrical resistivity anomalies in the southern part of the incised valley. Locations of the survey lines are presented in Figure 4A. (D) Topographic map showing the fault zone interpreted from the electrical resistivity and gravity surveys of this study.

(Figure 5) to obtain a high-resolution across-fault (ENE–WSW-trending) section in the southern part of the incised valley, which is interpreted from our gravity-survey results as a localized deformation zone along the eastern margin of the incised valley.

5.1 Data acquisition and inversion method

For the electrical resistivity investigation, two survey lines were installed to cross the presumed fault line. The length of the survey line was 1,900 m, with an electrode spacing of 20 or 40 m, and dipole–dipole and modified pole–pole arrays were applied to the electrode layout. As the dipole–dipole array gives a high resolution for vertical structures such as fault zones, and the modified pole–pole array has a high signal/noise (S/N) ratio for surrounding noise such as from artificial structures, field data were obtained using the two types of electrode array on the same survey line. A number of stainless steel electrodes were installed on the survey lines. These electrodes were connected to the main resistivity unit (Syscal Pro, IRIS Inc.) using connecting cables, and a current was flowed into the ground using current electrodes to measure and record

the potential difference between the potential electrodes. Before measuring the potential difference, the contact resistance of the electrodes and the ground was checked and adjusted so that their fluctuations were not large on the same survey line.

The commercially available DIPRO resistivity software (Heesong Geotek, 2002), developed by us, was used to determine a two-dimensional resistivity model for the subsurface using data obtained from the electrical resistivity survey. Figure 5A shows a flow diagram to obtain the 2D electrical resistivity through the inversion method using the data measured in the field. When making the initial 2D basin model, potential decay curves were drawn on the DIPRO resistivity software using all raw data, and some data with low S/N ratios were deleted. Five layers and a maximum depth of 100 m were assumed for the initial 2D basic models of the inversion. The vertical and horizontal mesh sizes were both 5 m divided into four meshes per measurement spacing. Inversion divided the surfaces into a number of small rectangular blocks, from which the resistivity values of the block were determined. The inversion routines applied were based on the smoothness-constrained least-squares optimization technique (Yi et al., 2001; Yi et al., 2003). Forward resistivity calculations involved

applying a finite-element-method (FEM)-based iterative algorithm. An error minimization method of L2 norm and fifth iteration were conducted to obtain sufficient convergence of the inversion error values. The RMS errors of each line range from 0.058 to 0.091.

5.2 Results and interpretation

Figures 5B, C shows the resultant electrical resistivity sections, namely, inversion results for survey lines 1 and 2, respectively. Figure 5B (survey line 1) can be divided into three horizontal layers. Within a depth of approximately 10 m from the surface, the electrical resistivity is greater than 100 Ω m and is interpreted as a gravel layer of a river bed. At a depth of approximately 10–60 m, the electrical resistivity is less than 80 Ω m and is inferred to be composed of sand strata and weathered soil–basement rock. The lowest part of the section at a depth of approximately 60–70 m has electrical resistivity values of more than 100 Ω m and is interpreted to be basement rock. The electrical resistivity section of survey line 2 (Figure 5C) was installed along the river bed, and the electrical potential difference was measured in a noisy environment caused by nearby dwellings and artificial structures. Therefore, inversion analysis was performed using the data obtained with the modified pole–pole array with a relatively high S/N ratio. Although the distribution of electrical resistivity is not layered like the result for survey line 1, the section for line 2 can be divided into unconsolidated strata, weathered soil–basement rock, and basement rock, with an electrical resistivity of 100 Ω m as the boundary.

The electrical resistivity of the ground depends on the stratum medium (rock types), porosity, electrical conductivity of pore water, water content, clay contents, and so on. Therefore, the fault zone shows a low resistivity because of its high water contents within the clay-rich fault gouges and breccias. The distribution of electrical resistivity in the two sections reveals regions interpreted as highly faulted zones at depth ranges of 1,420–1,480 m (survey line 1) and 1,340–1,400 m (survey line 2). Low resistivities of 40 Ω m or less show a vertical pattern, similar to the pattern shown in the fracture zone of the southern Yangsan Fault (Lee et al., 2017). Several weak electrical anomalies to the west of the lowest resistivities of the sections could be interpreted as minor fractured/deformed structures. We consider that the lowest resistivity values along the western front of the mountain range represent a N–S-oriented fault zone. This fault zone interpreted from the resistivity distribution shows a strong spatial correspondence with data obtained from our gravity survey and field observations of Quaternary fault exposures (Figure 5D). In here, we do not consider the Quaternary faulting records only based on the low electrical resistivities because of its resolution issue.

6 Discussion

6.1 Configuration and geometry of NNW–SSE-striking faults

Integrated results of our gravity and electrical surveys with field observations allow us to construct a comprehensive structural map showing the distribution of exposed and buried faults (Figure 6A). Our new findings reveal different distributions of faults in the southern and northern parts of the incised valley. In the southern part of the incised

valley, whose bedrock consists of Cretaceous sedimentary rocks, the fault displays a narrow deformation zone along the eastern margin of the valley. This deformation zone corresponds spatially with reverse-fault strands mapped by field observations along the mountain front. Surface ruptures generated during neotectonic earthquakes have been reported at two sites along these fault strands. Some low electrical anomalies to the west of these strands identified in both previous investigations and this study could be interpreted as subsidiary faults or shear fractures (Figures 5B–D), but we infer that the intensity of deformation to the west is much lower than that of the eastern marginal part of the valley. All of these results indicate that in the southern part of the valley, tectonic deformation is concentrated along a narrow zone in the southern part of the valley. In contrast, in the northern part of the valley, whose bedrock is composed of Late Cretaceous to Paleogene granitic rocks, multiple subparallel and interconnected faults are distributed within a wide zone of deformation. The northern distributed and complex deformation zone is also apparent in the reflection seismic survey results of Lee et al. (2000). Here, we note that, similar to the southern part of the valley, faults located along the eastern margin of the northern part of the valley correspond spatially to reverse-slip fault strands along the mountain front.

The width of the fault zone increases noticeably where the lithology of fault-hosting rocks changes from Cretaceous basement rocks in the south to granite in the north, and where the fault intersects with other major structures, namely, the Dongnae Fault in the west and the YTL in the east. In addition, the northern part of the fault zone could be wider than the southern part because of its intersection with the Yangsan Fault. Furthermore, the fault-zone width may also have been partially controlled by the differential susceptibility of rocks to erosion, with the northern part composed of granite hosting distributed faults and fractures.

6.2 Definition and characteristics of the Ulsan Fault Zone

Our data reveal that the NNW–SSE-striking fault zone is composed of multiple subparallel fault strands, even though its width varies along the fault strike, and its eastern boundary is characterized by the consistent presence of reverse-slip fault strands. Given this spatial distribution of faults, and with respect to previous concepts of the structure of the fault and valley, here we suggest that the term “Ulsan Fault Zone” can be defined as several interacting NNW–SSE-to N–S-striking fault strands within the incised valley and along the eastern margin of the valley (western front of the mountain range), extending from Gyeongju to Ulsan cities (Figure 6A).

Fault strands on the two sides of the Ulsan Fault Zone show variation in their predominant geometry, that is, their dip angle and kinematics. Faults along the eastern margin of the valley generally exhibit moderate-to low-angle dips (20°–65°) and mainly reverse-slip sense (Table 1; e.g., Kim et al., 2020b; Kim et al., 2021c; Gwon et al., 2021; Naik et al., 2022). Here, we discuss why the eastern edge of the Ulsan Fault Zone shows different features from the western edge and the potential relationship of the fault zone with the YTL. The YTL is located <3 km east of the reverse-slip fault traces along the mountain front (Figures 1B, C). During the Miocene crustal deformation, it acted as a dextral principal displacement zone (Kim et al., 1998; Son et al., 2002; Son et al., 2013; Son et al., 2015). It is also

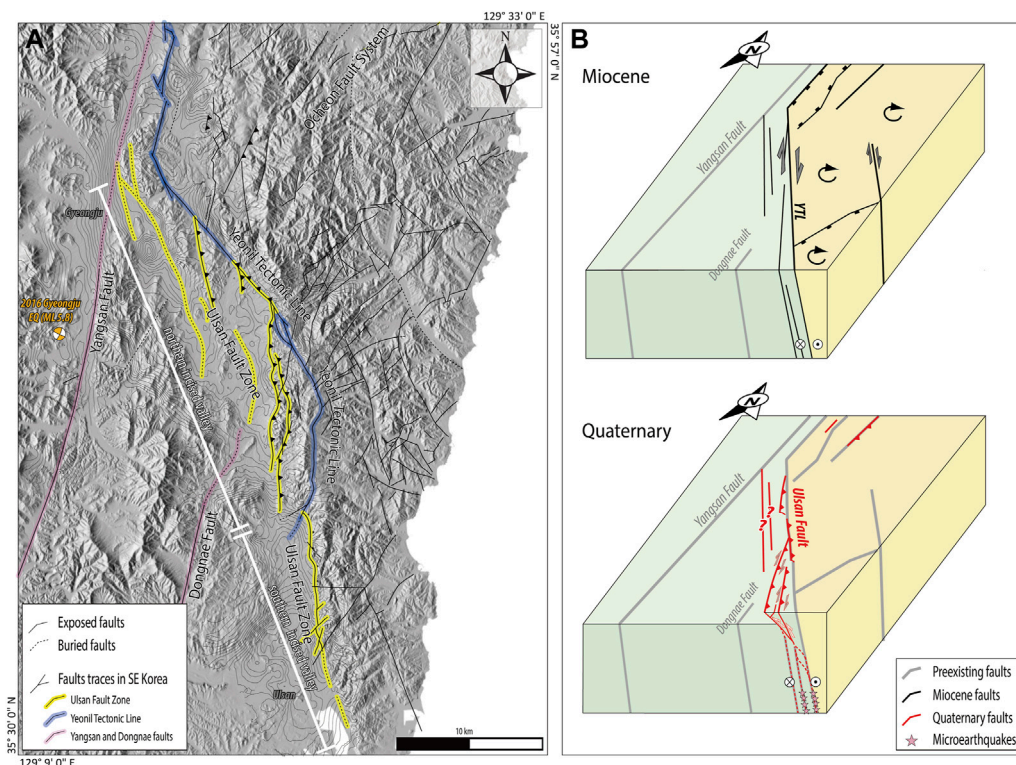


FIGURE 6 (A) Integrated map showing the configuration of the main faults in SE Korea, including the Ulsan Fault Zone, the YTL, and the Yangsan Fault. (B) Schematic block diagrams showing the spatiotemporal evolution of the Ulsan Fault Zone and YTL during the Miocene to Quaternary. See Section 6.3 for a detailed explanation.

noted that the clockwise rotation of crustal blocks occurred only in the block to the east of the YTL during the Early Miocene, as indicated by structural data (orientation variation of 48 Ma mafic dikes) and paleomagnetic observations [remanent magnetization directions of Early Miocene rocks and surrounding basement rocks; see figure 9 in [Son et al. \(2015\)](#) and references therein]. [Han et al. \(2017\)](#) documented microseismicity in our study area, and the locations of micro-earthquakes are spatially coincident with NNW–SSE-to N–S-striking faults. Those authors analyzed microearthquakes in continuous seismic data recorded between 2010 and 2014 and identified four NNW–SSE-to N–S-striking clusters of high-resolution seismicity. The most prominent of these clusters, which shows N–S-oriented and subvertically aligned hypocenters at depths of 8–11 km, is located less than 1 km east of the exposed reverse-fault trace (i.e., just east of the eastern gravity anomaly in the northern part of the incised valley). The other seismic clusters distributed to the east of the YTL also show high-to moderate-angle dips to the east at depths of 11–13 km. These features suggest that the reverse-slip strands along the eastern edge of the Ulsan Fault Zone showing moderate to low dip angles in the shallow subsurface region probably extended to deeper parts as high-angle dipping structures (>70° east) and that they developed as footwall shortcut thrusts (e.g., [McClay and Buchanan, 1992](#); [Butler et al., 2006](#); [Pace et al., 2014](#)) that nucleated from the shallow part of high-angle faults such as the YTL ([Kim et al., 2023](#)).

It is considered that neotectonic earthquakes have occurred along the inherited structures in the eastern part of the Ulsan

Fault Zone, but it is unclear whether such earthquakes have occurred in the western part. We suspect that some branched, steeply dipping strands within the northern part of the incised valley could be active faults that formed local areas of uplift within the incised valley, as inferred from the two streams flowing in opposite directions ([Figure 1C](#)) and abrupt changes in the depth of the unconformity between the unconsolidated strata and basement rocks observed from drilling data.

6.3 Spatiotemporal tectonic evolution of the Ulsan Fault Zone and adjacent major structures

Integrated results of our geophysical data and previous field observations support the concept of the Ulsan Fault Zone within the incised valley–mountain front in SE Korea ([Figure 6A](#)). In this section, we examine the spatiotemporal relationships between the Ulsan Fault Zone and the two adjacent major structures, namely, the YTL and the Yangsan Fault.

- (1) Ulsan Fault Zone–YTL: On the basis of the configuration, geometry, movement ages, and kinematics of the Ulsan Fault Zone and the YTL, we constructed a model of the long-term evolution of these two fault zones for the Miocene to Quaternary ([Figure 6B](#)). We propose that NNW–SSE-striking high-angle faults acted as dextral-slip faults that formed coevally with the back-arc opening of the East Sea

during the Miocene (Figure 6B; e.g., Son et al., 2002, 2005; Son et al., 2013; Son et al., 2015; Yoon et al., 2014; Kim et al., 2020a). Of these faults, the YTL played a key role as the principal western displacement zone bordering the Miocene sedimentary basins. The other faults, located to the west of the YTL, were probably subsidiary faults at that time and formed mainly as Riedel shears. Subsequently, during the neotectonic regime, some fault strands (or sections) along the YTL and nearby subsidiary faults were reactivated under an ENE–WSW maximum horizontal stress field, forming an imbricate thrust zone expressed as east-side-up geometry with reverse kinematics (Figures 6A, B). These reactivated faults with low to moderate dip angles developed as shortcut faults in the footwalls of pre-existing high-angle faults (Kim et al., 2023) owing to the combined effect of the imposed tectonic stress and fault attitudes as well as the low confining pressure in the shallow subsurface region.

- (2) Ulsan Fault Zone–Yangsan Fault: Our gravity-survey results reveal that the westernmost strand of several buried strands in the northern part of the incised valley, one of the constituent faults of the Ulsan Fault Zone, terminates by curving into the Yangsan Fault, showing a λ -type geometry in the vicinity of Gyeongju City (Figure 6A; Park, 2004; Han et al., 2009). Although the resolution of the image of the structural pattern obtained from the gravity survey limits the certainty of our interpretation, the inferred fault intersection suggests that the NNW–SSE-striking strand terminates at the prominent mature Yangsan Fault. In addition, there are no prominent NNW–SSE-striking structures to the west of the Yangsan Fault, and the NNW–SSE-striking western boundary faults of the Miocene Pohang Basin, which is adjacent to the YTL, are distributed only a few kilometers east of the Yangsan Fault (Figure 1B). These features indicate that the Ulsan Fault Zone formed in a later stage or deformation than formation of the mature Yangsan Fault. We conclude that the more distributed pattern of deformation in the northern part of the incised valley relative to the southern part is probably related to the structural complexity within the intersection area between these two major fault zones. This interpretation is supported by recent studies on the structural evolution of SE Korea, which have identified multiple stages of movement on the Yangsan Fault since at least the Late Cretaceous, with the most intense phase (dextral movement) occurring during the Paleogene (e.g., Ha et al., 2016; Cheon et al., 2019), and the subsequent development of Miocene sedimentary basins, which are distributed only to the east of the Yangsan Fault (e.g., Sohn and Son, 2004; Son et al., 2013; Son et al., 2015).

7 Conclusion

Based on integration of geological and geophysical (gravity and electrical resistivity) data, we focused on the structural architecture of the Ulsan Fault Zone, which is expressed as an NNW–SSE-striking incised valley–mountain range in SE Korea, and its late Cenozoic evolution. Our major conclusions are as follows.

- (1) The Ulsan Fault Zone is defined as a NNW–SSE-to N–S-striking fault within the incised valley and along the eastern margin of the valley. The incised valley can be divided into the northern distributed and complex deformation zone and the southern

concentrated deformation zone. Different deformation features between the two parts are controlled by the lithology of bedrocks and by the location and geometry of the adjacent major structures, such as, the YTL and the Yangsan Fault. Along the eastern margin of the valley, the constituent strands distributed have acted mainly as an imbricate thrust zone, showing an east-side-up geometry with moderate to low dip angles and reverse-dominant kinematics in the shallow subsurface, during the Quaternary.

- (2) The Quaternary reactivated strands within the Ulsan Fault Zone are interpreted as shortcut faults developed in the footwall of the Miocene subvertical structures, predominantly the YTL. In addition, movements on the Ulsan Fault Zone and the YTL during the Miocene to Quaternary were arrested by the NNE–SSW-striking Yangsan Fault. These spatial and temporal structural patterns of faulting in SE Korea suggest that the configuration of inherited structures strongly controlled the distribution and characteristics (i.e., geometry and kinematics) of subsequent crustal deformation during the late Cenozoic.

Data availability statement

The original contributions presented in the study are included in the article/Supplementary Material, further inquiries can be directed to the corresponding author.

Author contributions

YC: conception and design of the study, analysing and synthesizing structural data, writing the original draft; YS: performing and analysing gravity survey data, writing the section of original draft; SP: analysing electrical resistivity survey data, writing the section of original draft; J-HC: conception and design of the study, reviewing and editing the draft, funding acquisition; D-EK: analysing geomorphic data, writing the section of original draft; KK: performing electrical resistivity survey, funding acquisition; C-RR, Y-SK, and MS: analysing structural data, reviewing and editing the draft. All authors contributed to the article and approved the submitted version.

Funding

This work was supported by a grant from the Basic Research Project (GP 2020-014) of the KIGAM funded by the Korean Ministry of Science and ICT, by a grant (2022-MOIS62-001) for National Disaster Risk Analysis and Management Technology in Earthquakes funded by the Ministry of Interior and Safety (MOIS, South Korea), and by a grant (RS-2023-00255130) funded by the Korean Ministry of Ocean and Fisheries (South Korea).

Conflict of interest

The authors declare that the research was conducted in the absence of any commercial or financial relationships that could be construed as a potential conflict of interest.

Publisher's note

All claims expressed in this article are solely those of the authors and do not necessarily represent those of their affiliated

organizations, or those of the publisher, the editors and the reviewers. Any product that may be evaluated in this article, or claim that may be made by its manufacturer, is not guaranteed or endorsed by the publisher.

References

- Baag, C. E., and Kang, D. J. (1994). Geophysical studies on major faults in the Gyeongsang Basin: Aeromagnetic and radiometric data interpretation on the Ulsan Fault. *J. Geol. Soc. Korea* 30, 193–205.
- Becker, J. J., Sandwell, D. T., Smith, W. H. F., Braud, J., Binder, B., Depner, J., et al. (2009). Global bathymetry and elevation data at 30 arc seconds resolution: SRTM30_Plus. *Mar. Geod.* 32, 355–371. doi:10.1080/01490410903297766
- Blakely, R. J. (1995). *Potential theory in gravity and magnetic applications*. New York: Cambridge University Press. doi:10.1017/CBO9780511549816
- Butler, R. W. H., Tavarnelli, E., and Grasso, M. (2006). Structural inheritance in mountain belts: An Alpine–Apennine perspective. *J. Struct. Geol.* 28, 1893–1908. doi:10.1016/j.jsg.2006.09.006
- Chang, C.-J., and Chang, T. W. (1998). Movement history of the Yangsan Fault based on paleostress analysis. *J. Eng. Geol.* 8, 35–49.
- Chang, T. W. (2001). Quaternary tectonic activity at the eastern block of the Ulsan Fault. *J. Geol. Soc. Korea* 37, 431–444.
- Cheon, Y., Cho, H., Ha, S., Kang, H.-C., Kim, J.-S., and Son, M. (2019). Tectonically controlled multiple stages of deformation along the Yangsan Fault Zone, SE Korea, since Late Cretaceous. *J. Asian Earth Sci.* 170, 188–207. doi:10.1016/j.jseas.2018.11.003
- Cheon, Y., Choi, J.-H., Choi, Y., Bae, H., Han, K.-H., Son, M., et al. (2020b). Understanding the distribution and internal structure of the main core of the Yangsan Fault Zone: Current trends and future work. *J. Geol. Soc. Korea* 56, 619–640. doi:10.14770/jgsk.2020.56.5.619
- Cheon, Y., Choi, J.-H., Kim, N., Lee, H., Choi, I., Bae, H., et al. (2020a). Late Quaternary transpressional earthquakes on a long-lived intraplate fault: A case study of the southern Yangsan Fault, SE Korea. *Quat. Int.* 553, 132–143. doi:10.1016/j.quaint.2020.07.025
- Cheon, Y., Son, M., Song, C. W., Kim, J.-S., and Sohn, Y. K. (2012). Geometry and kinematics of the Ocheon Fault System along the boundary between the Miocene Pohang and Janggi basins, SE Korea, and its tectonic implications. *Geosci. J.* 16, 253–273. doi:10.1007/s12303-012-0029-0
- Cheong, C. S., Hong, D. G., Lee, K. S., Kim, J. W., Choi, J. H., Murray, A. S., et al. (2003). Determination of slip rate by optical dating of fluvial deposits from the Wangsan fault, SE Korea. *Quat. Sci. Rev.* 22, 1207–1211. doi:10.1016/S0277-3791(03)00020-9
- Choi, J.-H., Kim, Y.-S., Gwon, S., Edwards, P., Rezaei, S., Kim, T., et al. (2015). Characteristics of large-scale fault zone and Quaternary fault movement in Maegok-dong, Ulsan. *J. Eng. Geol.* 25, 485–498. doi:10.9720/kseg.2015.4.485
- Choi, J.-H. (2021) *Research in active tectonics and development of fault segment model for intraplate regions*. Daejeon, Korea: Korea Institute of Geoscience and Mineral Resources, 140.
- Choi, J.-H., Yang, S.-J., and Kim, Y.-S. (2009). Fault zone classification and structural characteristics of the southern Yangsan fault in the Sangcheon-ri area, SE Korea. *J. Geol. Soc. Korea* 45, 9–28.
- Choi, K. S., Yang, C. S., Shin, Y. H., and Ok, S. S. (2003). On the improvement of precision in gravity surveying and correction, and a dense Bouguer anomaly in and around the Korean Peninsula. *J. Korean Earth Sci. Soc.* 24, 205–215.
- Choi, P.-Y., Lee, C.-B., Ryo, C.-R., Choi, Y.-S., Kim, J.-Y., Hyun, H.-J., et al. (2002). Geometric analysis of the Quaternary Malbang fault: Interpretation of borehole and surface data. *J. Geol. Soc. Korea* 38, 163–174.
- Choi, S.-J., Jeon, J. S., Choi, J.-H., Kim, B., Ryo, C.-R., Hong, D.-G., et al. (2014). Estimation of possible maximum earthquake magnitudes of Quaternary faults in the southern Korean Peninsula. *Quat. Int.* 344, 53–63. doi:10.1016/j.quaint.2014.05.052
- Choi, S.-J., Jeon, J. S., Song, G. Y., Kim, H. C., Kim, Y. H., Choi, B. Y., et al. (2012). *Active fault map and seismic hazard map*. Seoul: Nat. Emergency Manag. Agency, 93.
- Choi, W.-H. (2003). Neotectonics of the Gyeongju-Ulsan area in the southeastern part of Korean Peninsula. Thesis of Ph.D. Korean: Seoul National Univ., 205.
- Chough, S. K., Kwon, S.-T., Ree, J.-H., and Choi, D. K. (2000). Tectonic and sedimentary evolution of the Korean peninsula: A review and new view. *Earth-Sci. Rev.* 52, 175–235. doi:10.1016/S0012-8252(00)00029-5
- Chough, S. K., and Sohn, Y. K. (2010). Tectonic and sedimentary evolution of a Cretaceous continental arc–backarc system in the Korean peninsula: New view. *Earth-Sci. Rev.* 101, 225–249. doi:10.1016/j.earscirev.2010.05.004
- DeMets, C., Gordon, R. G., Argus, D. F., and Stein, S. (1994). Effect of recent revisions to the geomagnetic reversal time scale on estimates of current plate motions. *Geophys. Res. Lett.* 21, 2191–2194. doi:10.1029/94GL02118
- Du, Y., and Aydin, A. (1995). Shear fracture patterns and connectivity at geometric complexities along strike-slip faults. *J. Geophys. Res.* 100, 18093–18102. doi:10.1029/95JB01574
- Engebretson, D. C., Cox, A., and Gordon, R. G. (1985). Relative motions between oceanic and continental plates in the Pacific Basin. *Geol. Soc. Am. Spec. Pap.* 206, 1–60. doi:10.1130/SPE206-p1
- Fabbri, O., Charvet, J., and Fournier, M. (1996). Alternate senses of displacement along the Tsushima fault system during the Neogene based on fracture analyses near the Western margin of the Japan Sea. *Tectonophysics* 257, 275–295. doi:10.1016/0040-1951(95)00151-4
- Farr, T. G., Rosen, P. A., Caro, E., Crippen, R., Duren, R., Hensley, S., et al. (2007). The shuttle radar topography mission. *Rev. Geophys.* 45, RG2004. doi:10.1029/2005RG000183
- Gwon, O., Park, K., Naik, S. P., Shin, H.-C., and Kim, Y.-S. (2021). A study on the characteristics of fault activity in the southern part of the Ulsan fault using paleoseismic method. *J. Geol. Soc. Korea* 57, 109–121. doi:10.14770/jgsk.2021.57.2.109
- Ha, S., Cheon, Y., Kang, H.-C., Kim, J.-S., Lee, S.-K., and Son, M. (2016). Geometry and kinematics of the subsidiary faults of the Ilgwang fault, SE Korea. *J. Geol. Soc. Korea* 52, 31–50. doi:10.14770/jgsk.2016.52.1.31
- Ha, S., Son, M., and Seong, Y. B. (2022). Active fault trace identification using a LiDAR high-resolution DEM: A case study of the central Yangsan Fault, Korea. *Remote Sens.* 14, 4838. doi:10.3390/rs14194838
- Hall, R. (2002). Cenozoic geological and plate tectonic evolution of SE Asia and the SW Pacific: Computer-based reconstructions, model and animations. *J. Asian Earth Sci.* 20, 353–431. doi:10.1016/S1367-9120(01)00069-4
- Han, M. H., Kim, K.-H., Kang, S. Y., and Son, M. (2017). Current microseismicity and generating faults in the Gyeongju area, southeastern Korea. *Tectonophysics* 694, 414–423. doi:10.1016/j.tecto.2016.11.026
- Han, S.-R., Park, J., and Kim, Y.-S. (2009). Evolution modeling of the Yangsan-Ulsan fault system with stress changes. *J. Geol. Soc. Korea* 45, 361–377.
- Heesong Geotek, H. (2002). *DIPRO for windows user's guide*. USA: Wintriss Controls Group, LLC.
- Heiskanen, W. A., and Vening Meinesz, F. A. (1958). *The Earth and its gravity field*. New York City: McGraw-Hill Book Co. Inc.
- Jolivet, L., Tamaki, K., and Fournier, M. (1994). Japan Sea, opening history and mechanism: A synthesis. *J. Geophys. Res. Solid Earth* 99, 22237–22259. doi:10.1029/93jb03463
- Kang, P.-C. (1979a). Geological analysis of landsat imagery of South Korea (I). *J. Geol. Soc. Korea* 15, 109–126.
- Kang, P.-C. (1979b). Geological analysis of landsat imagery of South Korea (II). *J. Geol. Soc. Korea* 15, 181–191.
- Kee, W. S., Kim, S. W., Hong, P. S., Lee, B. C., Cho, D. R., Byun, U. H., et al. (2019). *Geologic map of Korea (1:1,000,000)*. Daejeon, Korea: Korea Institute of Geoscience and Mineral Resources.
- Kim, H., Song, C.-W., Kim, J.-S., Son, M., and Kim, I.-S. (2008a). Tertiary geological structures and deformation history of the Southern Tsushima Island, Japan. *J. Geol. Soc. Korea* 44, 175–198.
- Kim, H., Synn, J.-H., Park, C., Song, W. K., Park, E. S., Jung, Y. B., et al. (2021). Korea stress map 2020 using hydraulic fracturing and overcoring data. *Tunn. Undergr. Space* 31, 145–166. doi:10.7474/TUS.2021.31.3.145
- Kim, I. S., Son, M., Jung, H. J., Lee, J. D., Kim, J. J., and Paik, I. S. (1998). Geological characteristics of Kyongju–Ulsan area: Palaeomagnetism and magnetic susceptibility of the granite rocks in the Ulsan fault area. *Econ. Environ. Geol.* 31, 31–43.
- Kim, J. H., Kang, P. C., and Lim, J. U. (1976). A study of the relation between geologic structures and ore deposits using Landsat-1 Images. *J. Geol. Soc. Korea* 2, 79–89.
- Kim, K. Y., Kim, D. H., and Lee, S. Y. (2008b). Near-surface geophysical studies in the Ulsan Fault Zone of Korea. *Explor. Geophys.* 39, 78–84. doi:10.1071/EG08008
- Kim, M.-C., Gihm, Y. S., Jeong, R. Y., Shinn, Y. J., and Son, M. (2020a). Site selection and characterization for onshore 10,000-ton-class CO₂ pilot storage in Early Miocene Janggi Basin, SE Korea: Storage potential and structural stability of siliciclastic-volcanic storage combination. *Int. J. Greenh. Gas. Control* 103, 103174. doi:10.1016/j.ijggc.2020.103174
- Kim, M.-C., Jung, S., Yoon, S., Jeong, R. Y., Song, C. W., and Son, M. (2016). Neotectonic crustal deformation and current stress field in the Korean peninsula and

- their tectonic implications: A review. *J. Pet. Soc. Korea* 25, 169–193. doi:10.7854/JPSK.2016.25.3.169
- Kim, N., Park, S. I., Cho, C. S., Cheon, Y., and Peace, A. L. (2023). Neotectonic transpressional intraplate deformation in Eastern Eurasia: Insights from active fault systems in the southeastern Korean Peninsula. *Geosci. Front.* 14, 101559. doi:10.1016/j.gsf.2023.101559
- Kim, N., Park, S. I., and Choi, J. H. (2021b). Internal architecture and earthquake rupture behavior of a long-lived intraplate strike-slip fault: A case study from the southern Yangsan Fault, Korea. *Tectonophysics* 816, 229006. doi:10.1016/j.tecto.2021.229006
- Kim, S. W. (1973). A study on the Terraces along the southeastern coast (Bangeogin-Pohang) of the Korean Peninsula. *J. Geol. Soc. Korea* 9, 89–121.
- Kim, T., Kim, D. E., Kim, S. J., Seong, Y. B., Lim, H. S., Shin, H. C., et al. (2021c). Kinematic characteristics and movement timing of the Wonwonsa fault in the central Ulsan fault. *J. Geol. Soc. Korea* 57, 35–48. doi:10.14770/jgsk.2021.57.1.35
- Kim, T., Shin, H. C., and Kim, Y. S. (2020b). Characteristics of the topographical deformation in the central part of the Ulsan fault. *J. Geol. Soc. Korea* 56, 193–209. doi:10.14770/jgsk.2020.56.2.193
- Kim, Y. S., Andrews, J. R., and Sanderson, D. J. (2000). Damage zones around strike-slip fault systems and strike-slip fault evolution, Crackington Haven, southwest England. *Geosci. J.* 4, 53–72. doi:10.1007/bf02910127
- Ko, K., Choi, S. J., Lee, T. H., Gihm, Y. S., Kim, C.-M., Kim, K., et al. (2022). A multidisciplinary approach to characterization of the mature northern Yangsan fault in Korea and its active faulting. *Mar. Geophys. Res.* 43, 21. doi:10.1007/s11001-022-09486-w
- Kuwahara, Y., Choi, J.-H., Cheon, Y., and Imanishi, K. (2021). Dependence of earthquake faulting type on fault strike across the Korean Peninsula: Evidence for weak faults and comparison with the Japanese Archipelago. *Tectonophysics* 804, 228757. doi:10.1016/j.tecto.2021.228757
- Kyung, J.-B. (1997). Paleoseismological study on the mid-northern part of Ulsan Fault by trench method. *J. Eng. Geol.* 7, 81–90.
- Lee, G.-R., Park, C.-S., and Shin, J.-R. (2018). Distribution of fault-related landforms and lineaments along the Ulsan Fault Zone. *J. Koran Geomorphol. Assoc.* 25, 89–103. doi:10.16968/JKGA.25.3.89
- Lee, G. H., Yoon, Y., Nam, B. H., Lim, H., Kim, Y.-S., Kim, H. J., et al. (2011). Structural evolution of the southwestern margin of the Ulleung Basin, East Sea (Japan Sea) and tectonic implications. *Tectonophysics* 502, 293–307. doi:10.1016/j.tecto.2011.01.015
- Lee, H. J., Hamm, S. Y., Park, S., and Ryoo, C. R. (2017). Geometric Characteristics of Southern Yangsan Fault Zone by Means of Geophysical Prospecting and Geological Survey. *J. Eng. Geol.* 27, 9–20. doi:10.9720/kseg.2017.1.9
- Lee, J.-H., Lee, J.-H., Yoon, S.-H., Lee, H.-S., Song, H.-Y., and Kim, G.-B. (2022). Two distinct back-arc closure phases of the East Sea: Stratigraphic evidence from the SW ulleung basin margin. *Front. Earth Sci.* 10, 839712. doi:10.3389/feart.2022.839712
- Lee, K.-J., Kim, K. Y., Kim, W.-H., and Im, C.-B. (2000). Seismic studies on velocity anisotropy in the ulsan Fault Zone. *J. Korean Geophys. Soc.* 3, 49–56.
- Lee, K., and Um, C. R. (1992). Geoelectric survey of the Ulsan Fault: Geophysical studies on major faults in the Kyeongsang basin. *J. Geol. Soc. Korea* 28, 32–39.
- Lee, S. R. (2020). *Research on geologic hazard assessment of large fault system-focusing on central region of the Yangsan fault*. Daejeon, Korea: Korea Institute of Geoscience and Mineral Resources, 229.
- Lee, Y. H. (2003). Quaternary faults in the eastern area of the Ulsan fault (Korea). Thesis of Master. Korea: Pusan National University, 74.
- Lee, Y. S., Ishikawa, N., and Kim, W. K. (1999). Paleomagnetism of tertiary rocks on the Korean peninsula: Tectonic implications for the opening of the East Sea (Sea of Japan). *Tectonophysics* 304, 131–149. doi:10.1016/S0040-1951(98)00270-4
- Lim, M., Shin, Y., Park, Y., Rim, H., Ko, I. S., and Park, C. (2019). Digital Gravity Anomaly Map of KIGAM. *Geophys. Geophys. Explor.* 22, 37–43. (in Korean with English abstract) 713. doi:10.7582/GGE.2019.22.1.037
- Lithgow-Bertelloni, C., and Richards, M. A. (1998). The dynamics of Cenozoic and Mesozoic plate motions. *Rev. Geophys.* 36, 27–78. doi:10.1029/97RG02282
- McClay, K. R., and Buchanan, P. G. (1992). “Thrust faults in inverted extensional basins,” in *Thrust Tectonics*. Editors K. R. McClay (Dordrecht: Springer). doi:10.1007/978-94-011-3066-0_8
- Naik, S. P., Gwon, O., Park, K., Bae, S. Y., Shin, H.-C., Choi, J.-H., et al. (2022). Localization and characterization of the southern Ulsan fault (UF) using geo-electrical imaging: Implication for seismic hazard assessment in an urbanized area. *J. Geodyn.* 151, 101919. doi:10.1016/j.jog.2022.101919
- O’Neill, C., Müller, D., and Steinberger, B. (2005). On the uncertainties in hot spot reconstructions and the significance of moving hot spot reference frames. *Geochem. Geophys. Geosys.* 6, 04003. doi:10.1029/2004GC000784
- Okada, A., Watanabe, M., Suzuki, Y., Kyung, J.-B., Jo, W.-R., Kim, S.-K., et al. (1998). Active fault topography and fault outcrops in the central part of the Ulsan fault system, southeast Korea. *J. Geogr.* 107, 644–658. doi:10.5026/jgeography.107.5_644
- Pace, P., Domenica, A. D., and Calamita, F. (2014). Summit low-angle faults in the central appennines of Italy: Younger-on-older thrusts or rotated normal faults? Constraints for defining the tectonic style of thrust belts. *Tectonics* 33, 756–785. doi:10.1002/2013TC003385
- Park, H.-J., Han, R., and Gu, D. (2020). Structures and deformation characteristics of the active fault, Hwalseongri area, Gyeongju, Korea. *J. Geol. Soc. Korea* 56, 703–726. doi:10.14770/jgsk.2020.56.6.703
- Park, J. Y. (2004). The structural characteristics of the Tertiary basin in Gyeongju region, Korea. Master thesis. Korea: Seoul National University, 128.
- Park, K., Naik, S. P., Gwon, O., Shin, H.-C., and Kim, Y.-S. (2022). Characterization of fault kinematics based on paleoseismic data in the Malbang area in the central part of the Ulsan Fault Zone. *J. Korean Earth Sci. Soc.* 43, 151–164. doi:10.5467/JKES.2022.43.1.151
- Park, Y., Ree, J.-H., and Yoo, S.-H. (2006). Fault slip analysis of Quaternary faults in southeastern Korea. *Gondwana Res.* 9, 118–125. doi:10.1016/j.gr.2005.06.007
- Ryoo, C.-R. (2009). A report for the Quaternary Gaegok 6 fault developed in the mid-eastern part of ulsan Fault Zone, Korea. *Econ. Environ. Geol.* 42, 635–643.
- Ryoo, C.-R., Chwae, U., Choi, S.-J., and Son, M. (2001). Quaternary faults in Hwalseong-ri, Oedong-eup, Gyeongju, Korea. *KIGAM Bull.* 5, 24–33.
- Ryoo, C.-R., Lee, B. J., and Chwae, U. (2000). Quaternary fault and its remote sensing image in the southeastern Korea. *CCOP Tech. Bull.* 29, 5–28.
- Ryoo, C.-R., Lee, B. J., Son, M., Lee, Y. H., Choi, S.-J., and Chwae, U. (2002). Quaternary faults in Gaegok-ri, Oedong-eup, Gyeongju, Korea. *J. Geol. Soc. Korea* 38, 309–323.
- Ryoo, C.-R., Son, M., Lee, Y. H., Choi, S.-J., and Chwae, U. (2004). Quaternary faults around Bulguk-sa, Gyeongju, Korea. *KIGAM Bull.* 8, 3–17.
- Saltus, R. W., and Blakely, R. J. (2011). Unique geologic insights from “non-unique” gravity and magnetic interpretation. *GSA Today* 21, 4–10. doi:10.1130/G136A.1
- Schellart, W. P., and Rawlinson, N. (2010). Convergent plate margin dynamics: New perspectives from structural geology, geophysics and geodynamic modelling. *Tectonophysics* 483, 4–19. doi:10.1016/j.tecto.2009.08.030
- Sohn, Y., Choi, S., and Ryu, I.-C. (2020). Gravity field interpretation for the deep geological structure analysis in Pohang-Ulsan, Southeastern Korean Peninsula. *Econ. Environ. Geol.* 53, 597–608. doi:10.9719/EEG.2020.53.5.597
- Sohn, Y. K., Ki, J. S., Jung, S., Kim, M.-C., Cho, H., and Son, M. (2013). Synvolcanic and syntectonic sedimentation of the mixed volcanoclastic-epiclastic succession in the Miocene Janggi Basin, SE Korea. *Sediment. Geol.* 288, 40–59. doi:10.1016/j.sedgeo.2013.01.002
- Sohn, Y. K., and Son, M. (2004). Synrift stratigraphic geometry in a transfer zone coarse-grained delta complex, Miocene Pohang Basin, SE Korea. *Sedimentology* 51, 1387–1408. doi:10.1111/j.1365-3091.2004.00679.x
- Shon, H., Yun, H., and Oh, J. (1999). Deep structure of Ulsan Fault by electric and EM surveys in Ipsil area, south of Kyeongju. *Econ. Environ. Geol.* 32, 161–167.
- Son, M., Chong, H.-Y., and Kim, I.-S. (2002). Geology and geological structures in the vicinities of the southern part of the Yonil Tectonic Line, SE Korea. *J. Geol. Soc. Korea* 38, 175–197.
- Son, M., Kim, I.-S., and Sohn, Y. K. (2005). Evolution of the Miocene Waup Basin, SE Korea, in response to dextral shear along the southwestern margin of the East Sea (Sea of Japan). *J. Asian Earth Sci.* 25, 529–544. doi:10.1016/j.jseaes.2004.06.003
- Son, M., Song, C. W., Kim, M.-C., Cheon, Y., Cho, H., and Sohn, Y. K. (2015). Miocene tectonic evolution of the basins and fault systems, SE Korea: Dextral, simple shear during the East Sea (Sea of Japan) opening. *J. Geol. Soc. Korea* 172, 664–680. doi:10.1144/jgs2014-079
- Son, M., Song, C. W., Kim, M.-C., Cheon, Y., Jung, S., Cho, H., et al. (2013). Miocene crustal deformation, basin development, and tectonic implication in the southeastern Korean Peninsula. *J. Geol. Soc. Korea* 49, 93–118.
- Song, M.-Y., and Kyung, J. B. (1996). A geophysical survey in the central part of the Ulsan Fault and determination of fault characteristics. *J. Korean Earth Sci. Soc.* 17, 205–212.
- Taira, A. (2001). Tectonic evolution of the Japanese island arc system. *Annu. Rev. Earth Planet. Sci.* 29, 109–134. doi:10.1146/annurev.earth.29.1.109
- Wada, S., Sawada, A., Hiramatsu, Y., Matsumoto, N., Okada, S., Tanaka, T., et al. (2017). Continuity of subsurface fault structure revealed by gravity anomaly: The eastern boundary fault zone of the niigata plain, central Japan. *Earth, Planets Space* 69, 15. doi:10.1186/s40623-017-0602-x
- Xu, X., Zuzza, A. V., Chen, L., Zhu, W., Yin, A., Fu, X., et al. (2021). Late Cretaceous to Early Cenozoic extension in the Lower Yangtze region (East China) driven by Izanagi-Pacific plate subduction. *Earth-Sci. Rev.* 221, 103790. doi:10.1016/j.earscirev.2021.103790
- Yi, M. J., Kim, J. H., and Chung, S. H. (2003). Enhancing the resolving power of least-squares inversion with active constraint balancing. *Geophysics* 68, 931–941. doi:10.1190/1.1581045
- Yi, M. J., Kim, J. H., Song, Y. H., Cho, S. J., Chung, S. H., and Suh, J. H. (2001). Three dimensional imaging of subsurface structures using resistivity data. *Geophys. Prospect.* 49, 483–497. doi:10.1046/j.1365-2478.2001.00269.x
- Yin, A. (2010). Cenozoic tectonic evolution of Asia: A preliminary synthesis. *Tectonophysics* 488, 293–325. doi:10.1016/j.tecto.2009.06.002
- Yoon, S. H., Sohn, Y. K., and Chough, S. K. (2014). Tectonic, sedimentary, and volcanic evolution of a back-arc basin in the East Sea (Sea of Japan). *Mar. Geol.* 352, 70–88. doi:10.1016/j.margeo.2014.03.004